

# Optical Spectra of Small-scale Sprite Features Observed at 10,000 fps

Hans C. Stenbaek-Nielsen<sup>1</sup>, Matthew G McHarg<sup>2</sup>, Ryan Haaland<sup>3</sup>, and Alejandro Luque<sup>4</sup>

<sup>1</sup>University of Alaska Fairbanks

<sup>2</sup>US Air Force Academy

<sup>3</sup>Augsburg College

<sup>4</sup>Institute for Astrophysics of Andalusia (IAA-CSIC), in Granada, Spain

November 22, 2022

## Abstract

Spectra of small-scale sprite structures, downward and upward propagating streamers, glow, and beads, were recorded with a slit-less spectrograph at 10,000 frames per second (fps) from aircraft missions in 2009 and 2013. The spectra are dominated by emissions from molecular nitrogen, the 1 positive band in the red, and in the blue the 2 positive band plus the 1 negative band of molecular nitrogen ions. The excitation threshold for the blue emissions is higher than for the red emissions so the blue/red ratio can, in principle, be used as a proxy for the electron energy leading to the emissions. We extracted for analysis time series of spectra from 11 sprites: 18 time series from downwards propagating streamers, 6 from upward propagating streamers, 14 from glow and 12 from beads. The total number of spectra in the 50 time series is 953. Blue emissions are almost exclusively associated with streamers indicating the more energetic nature of streamers compared with glow and beads. Both downward and upward propagating streamers start and end with low blue emissions indicating time variations in the associated processes. Because the red and blue nitrogen emissions are significantly affected by quenching, which is altitude dependent, and we do not have sufficiently accurate altitudes, the observed spectral blue/red ratios cannot be directly applied to sprite models.

1  
2  
3  
4  
5  
6  
7  
8  
9  
10  
11  
12  
13  
14  
15  
16  
17

## **Optical Spectra of Small-scale Sprite Features Observed at 10,000 fps**

**H.C. Stenbaek-Nielsen<sup>1</sup>, M.G. McHarg<sup>2</sup>, R. Haaland<sup>3</sup>, A. Luque<sup>4</sup>**

<sup>1</sup> University of Alaska Fairbanks, Fairbanks, Alaska, USA.

<sup>2</sup> US Air Force Academy, Colorado Springs, Colorado, USA.

<sup>3</sup> Augsburg University, Minneapolis, Minnesota, USA.

<sup>4</sup> Instituto de Astrofísica de Andalucía (IAA), CSIC, Granada, Spain.

Corresponding author: H.C. Stenbaek-Nielsen (hcnielsen@alaska.edu)

### **Key Points:**

- Spectra of small scale sprite features (downward and upward streamers, beads and glow) have been recorded at 10,000 spectra per second.
- The spectra are dominated by molecular nitrogen emissions. The relative blue and red emission rates can be used to assess the processes leading to the emissions.
- Blue emissions are almost exclusively associated with sprite streamers indicating more energetic processes compared to those associated with beads and glow.

## 18 **Abstract**

19 Spectra of small-scale sprite structures, downward and upward propagating streamers, glow, and  
20 beads, were recorded with a slit-less spectrograph at 10,000 frames per second (fps) from aircraft  
21 missions in 2009 and 2013. The spectra are dominated by emissions from molecular nitrogen, the  
22 1<sup>st</sup> positive band in the red, and in the blue the 2<sup>nd</sup> positive band plus the 1<sup>st</sup> negative band of  
23 molecular nitrogen ions. The excitation threshold for the blue emissions is higher than for the red  
24 emissions so the blue/red ratio can, in principle, be used as a proxy for the electron energy  
25 leading to the emissions. We extracted for analysis time series of spectra from 11 sprites: 18 time  
26 series from downwards propagating streamers, 6 from upward propagating streamers, 14 from  
27 glow and 12 from beads. The total number of spectra in the 50 time series is 953. Blue emissions  
28 are almost exclusively associated with streamers indicating the more energetic nature of  
29 streamers compared with glow and beads. Both downward and upward propagating streamers  
30 start and end with low blue emissions indicating time variations in the associated processes.  
31 Because the red and blue nitrogen emissions are significantly affected by quenching, which is  
32 altitude dependent, and we do not have sufficiently accurate altitudes, the observed spectral  
33 blue/red ratios cannot be directly applied to sprite models.

## 34 **1 Introduction**

35 Optical spectra of sprites, first obtained by Mende et al. (1995); Hampton et al. (1996),  
36 are dominated by molecular nitrogen band emissions: The First Positive band system (1PN2) in  
37 the red and in the blue the Second Positive band system (2PN2) and the first Negative band  
38 system of molecular nitrogen ions (1NN2+). The excitation threshold for the first and second  
39 positive system is 7.4 eV and 11.0 eV, respectively, while ionization requires 15.6 eV  
40 (Cartwright, 1978; Vallance Jones, 1974). The emissions are very bright and they are readily  
41 identifiable in spectra recorded at 10,000 frames per second (Kanmae et al., 2010a), and  
42 therefore may be used to evaluate the temporal development of the characteristic energy of the  
43 electrons leading to the emissions.

44 The use of spectral features to evaluate the causal processes is not new. Suszcynsky et al.  
45 (1998) and Armstrong et al. (2000) compared emissions in the 380-450 nm region (blue), to  
46 emissions in the 600-900 nm region (red) and suggested that there are two separate mechanisms  
47 associated with the sprite emissions: An initial energetic process followed by less energetic  
48 processes. The observations were made from aircraft using photometers together with 30 fps  
49 video cameras. Morrill et al. (2002), also using aircraft data, found that emissions in sprite  
50 streamers indicate higher electron energies at lower altitudes. Similarly, Kuo et al. (2005) and  
51 Liu et al., (2006 and 2009a) used data from a spectrophotometer onboard the FORMOSAT-2  
52 satellite to derive the characteristic electron energies and associated ambient electric fields. More  
53 recently, Gordillo-Vázquez et al. (2018) used sprite spectra with 0.24 nm resolution to derive  
54 mesospheric temperatures and found no measurable heating of the neutral atmosphere. Finally,  
55 modeling by Pérez-Invernón et al. (2018) indicate that the ratio of 1PN2 to 2PN2, the emissions  
56 that dominate the 10,000 frames per second observations presented in this paper, does not vary  
57 much for reduced electric fields above ~200 Td, but is adequate at lower fields. They suggest  
58 that a better ratio might be 1PN2 or 2PN2 to 1NN2+.

59 Sprites develop on millisecond time scales, and they have complex spatial structures with  
60 scale sizes down to a few 10s of meters. This obviously places severe limitations on observations  
61 made with traditional photometers and 30 fps video cameras. Fortunately, sprites are very bright,

62 and therefore most of these limitations were overcome once high-speed imaging became  
63 available. Using high-speed imaging it is possible to observe sprites with sufficient temporal and  
64 spatial resolution to document details of sprite morphology (e.g. Stanley et al., 1999; Stenbaek-  
65 Nielsen et al., 2000; Cummer et al., 2006; McHarg et al., 2007; Stenbaek-Nielsen & McHarg,  
66 2008; Stenbaek-Nielsen et al., 2013).

67 Sprite spectra with 3 ms temporal resolution were recorded in 2005 with a slit  
68 spectrograph (Kanmae et al., 2007). During the same 2005 campaign images were also recorded  
69 at 10,000 fps (0.1 ms temporal resolution). The images showed that sprite streamers are fast  
70 moving, small-scale, but very bright, features (Stenbaek-Nielsen et al., 2007). This makes them  
71 well suited for slit-less spectroscopy, and in 2009 sprite spectra using this technique were  
72 recorded at 10,000 fps (Kanmae et al., 2010a). While the slit-less spectra have less spectral  
73 resolution than those recorded with the slit spectrograph, spectra can be recorded within a much  
74 larger field of view, and spectra can be obtained of streamers as they propagate across the field  
75 of view. This will allow an investigation of temporal changes to the spectra.

76 Both the 2005 and the 2007 observations were made from the ground. Contrary to  
77 expectations, no blue emissions were detected, and it was suggested that the reason was  
78 absorption and scattering in the lower atmosphere. The 2009 spectra were recorded from an  
79 aircraft at high altitude, and, indeed, emissions in the blue were detected. Evaluating these  
80 observations Kanmae et al. (2010b) showed the more energetic nature of streamers compared to  
81 glows. A second similar aircraft mission was conducted in 2013.

82 There are many dynamic and bright small-scale features in sprites which are ideally  
83 suited for high-speed slit-less spectroscopy, and in this paper we present an analysis of spectra  
84 obtained at 10,000 fps in the 2009 and 2013 aircraft sprite missions. We evaluate nitrogen  
85 emissions in the blue and red from 4 sprite features: downward and upward propagating  
86 streamers, sprite glow, and beads. Streamers are mainly observed in the initial phase of a sprite  
87 event while glow and beads are longer lasting and largely stationary. Glow and beads are  
88 typically the main sprite features in video recordings (30 or 25 fps).

89 The spectra are dominated by molecular nitrogen emissions. Most of the spectra have a  
90 well-defined spectral signature between 625 and 700 nm in the red. This is the  $\Delta v=3$  bands in the  
91 1<sup>st</sup> positive system of molecular nitrogen. While they are generally less bright than the  $\Delta v=2$   
92 bands in the 720-780 nm range, they are better defined in our data, and we use them as primary  
93 selection criterion when selecting events. The wavelength range used for the blue emissions is  
94 380-450 nm, which covers part of the 2P system of molecular nitrogen and molecular nitrogen  
95 ions. The 380 nm limit is the spectrograph low wavelength cut-off, and therefore only the longer  
96 wavelength bands of the 2P system will be detected. The spectrograph does not have enough  
97 resolution to fully separate 2PN2 and molecular nitrogen ion emissions, but since both require  
98 higher energies to emit than the 1PN2 band, alone the presence of blue in the spectra will  
99 indicate a more energetic process.

100 The nitrogen emissions are affected by quenching (deactivation of the excited molecules  
101 by atmospheric collisions rather than through photon emissions). Hence, if the observed  
102 emissions are to be used with models to infer the characteristic electron energies involved, which  
103 would be an obvious next step, the emissions have to be corrected for quenching. Quenching is  
104 altitude dependent, and there is unfortunately a substantial uncertainty on the altitudes of the  
105 emitting sprite features which, in effect, prevents the observations to be used quantitatively with

106 models to infer the characteristic electron energies involved. We discuss this in detail in sections  
107 4.1 and 4.2 below. Nevertheless, the ratio of blue to red emissions derived from our observed  
108 spectra is a convenient parameter for an evaluation of systematic differences between the 4  
109 small-scale sprite features. In section 4.3 we present ratio averages across the entire data set, and  
110 in section 4.4 temporal changes observed within individual spectral time series.

## 111 **2 Instrumentation**

112 Essentially the same slit-less spectrograph was used in the 2009 and 2013 recordings at  
113 10,000 fps. It was configured with a 100 lines/mm transmission grating blazed at 425 nm in front  
114 of a Nikon 50 mm f/1.4 lens on a Video Scope VS4-1845HS image intensifier. The extended  
115 blue response intensifier has a P24 phosphor (10  $\mu$ s decay) preventing persistence onto following  
116 images. The intensified spectral image is relayed to the CMOS chip of a Vision Research  
117 Phantom high-speed camera. The Phantom camera uses GPS time, and it is configured and  
118 controlled by a laptop computer which is also used for the storage of events initially recorded in  
119 camera memory.

120 In 2009 we used a Phantom v7.1, which has 12 bit images, and in 2013 an improved  
121 Phantom v7.3 with 14 bit images. Both models use the same 800x600 pixel format CMOS chip,  
122 but at 10,000 fps hardware limitations reduce the usable image size. For the v7.1 (2009) we  
123 configured the Phantoms to 640x256 and for the v7.3 (2013) to 640x320 pixel image formats,  
124 corresponding to a field of view of 15x6 and 15x7.5 degrees respectively.

125 The spectrograph was mounted on an adjustable azimuth-elevation mount looking out  
126 through one of the left side windows on the aircraft. Co-mounted with the spectrograph we had a  
127 low light-level video camera (Watec 902H) to provide scene awareness and to record star  
128 background critical for accurate pointing information. On a separate mount, looking through  
129 another window, we had a second Phantom camera configured as an imager and a co-mounted  
130 Watec video camera, but these data were not used directly in the analysis presented here.

131 The spectrograph was wavelength calibrated using an Ocean Optics HG-1 Mercury  
132 Argon Calibration Source. The dispersion is 4.05 nm/pixel, and it varies only slightly across the  
133 field of view. During the missions we recorded spectra of a number of bright stars with known  
134 spectra. Analysis of the 2009 spectra shows a response across the visible and near-IR from 380  
135 to 900 nm with a steep fall off in the blue and a peak response around 550 nm (Kanmae et al.,  
136 2010b). In the 2013 mission we looked through a quartz window expecting better response in the  
137 blue, but that was not the case, and we found the blue cut-off is primarily due to the transmission  
138 characteristics of the Nikon 50 mm lens. While the blue response in the 2013 mission was  
139 slightly better we did not find in the analysis any material differences between the spectra from  
140 the 2009 and the 2013 missions.

141 Most of the molecular nitrogen 2P bands emits at shorter wavelengths than the 380 nm  
142 instrument cut-off, which is unfortunate. On the other hand, the 2P bands are bright, and the cut-  
143 off prevents 2<sup>nd</sup> order spectra to interfere with the 1<sup>st</sup> order spectra which simplifies analysis  
144 considerably.

145 Getting the spectral information with slit-less spectroscopy requires small sources,  
146 ideally, as in astronomy, point sources. In that case the resolution would be 4.05 nm/pixel. While  
147 the sprite structures analyzed here are small, they are not point sources and the spectral  
148 resolution would be less. The structures are typically 3 to 10 pixels wide and the resolution

149 would then be ~15-40 nm. This is not sufficient for a clear separation of the neutral and ion  
150 emissions in the blue, but acceptable when we just want to isolate the signals in the wavelength  
151 regions of the 1PN2 and 2PN2 bands.

152 With the 100 lines/mm grating first order spectra covering 0 to 800 nm are ~200 pixels  
153 wide, which is ~1/3 of the 640 pixel image width. On one of the flights in 2009 we used a 200  
154 lines/mm grating to provide twice the spectral resolution, but the wider spectra (in pixels)  
155 significantly reduces the area in the image from which spectra can be recorded, and it resulted in  
156 an unacceptable loss of otherwise usable events.

### 157 **3 Data**

158 Sprites and their spectra were recorded at 10,000 fps in the 2009 and 2013 aircraft  
159 missions over the US mid-west region. Additionally, we recorded GPS aircraft position with 1 s  
160 temporal resolution, and lightning strikes from the National Lightning Detection Network  
161 (NLDN). A total of 60 sprites with spectra were recorded, but because of overlap of spectral  
162 features within an image, only relatively few events will produce spectra where the 1P (red) and  
163 2P (blue) bands from particular sprite features are sufficiently isolated to allow evaluation. Only  
164 2 of the 60 events were found to have all 4 sprite features, downward and upward propagating  
165 streamers, beads, and glow, present with spectra of sufficient quality for evaluation. However,  
166 there were a number of events with good spectra for 2 and 3 features thus allowing for a more  
167 statistical analysis.

168 For analysis we selected 11 events. An event was selected if it has usable spectra for at  
169 least 2 of the 4 sprite features in the analysis. The  $\Delta v=3$  band of the 1P system of molecular  
170 nitrogen is typically a well-defined feature in the spectra. It is observed between 625-700 nm,  
171 and we used that spectral feature as primary selection criteria. For each feature within an event  
172 we then extracted as many sequential spectra as possible to provide data for an evaluation of the  
173 temporal development of the blue and red emissions. The 11 events yielded 50 sequences of  
174 spectra, 18 of downward streamers, 6 of upward streamers, 14 of glows, and 12 of beads. The  
175 total number of spectra in the 50 sprite feature sequences is 953.

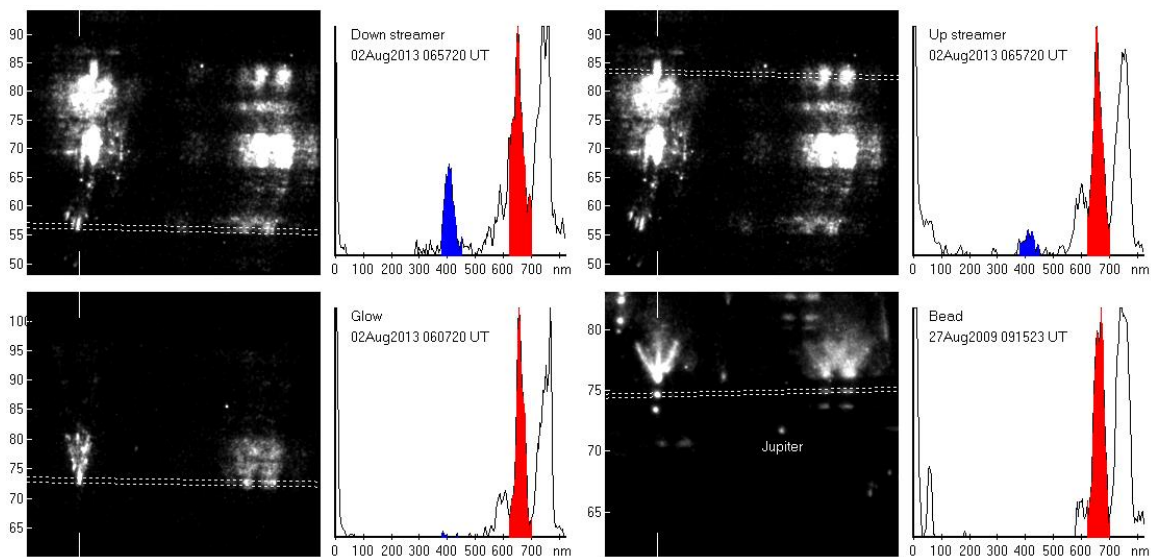
176 Most of the spectra were present against a dark background, but there were some where  
177 otherwise well-defined spectral features were observed against a relatively uniform background  
178 created, for example, by the presence of a sprite halo. In this case we used background  
179 subtraction to isolate the spectral features of interest.

180 The spectra are affected by the atmosphere and by noise originating primarily in the  
181 camera intensifier. To evaluate this we analyzed spectra from the planet Jupiter which was in the  
182 field of view in a sprite recorded on 27 August 2009 at 091523 UT. We extracted 200  
183 consecutive spectra, 0.02 s of data, and assuming that the emissions from Jupiter do not vary  
184 over the 0.02 s data sequence, the scatter in the brightness, which appears to be random, will  
185 reflect the uncertainty thus introduced on the data. To be consistent with the analysis presented in  
186 this paper, we evaluated the scatter for the same spectral bands, 380-450 nm in the blue and 625-  
187 700 nm in the red, used for the data analysis presented in this paper. Details of the procedure are  
188 given in section 4 below. The standard deviation in the red is 793 on a ~10,000 signal (8%) and  
189 for the blue 856 on a ~5,000 signal (19%). Following standard error analysis procedures (Taylor,  
190 1997), we will use the Jupiter data to estimate error bars on temporal variations in spectra from  
191 individual sprites presented in section 4.4 below.

192 **4 Analysis**

193 Figure 1 shows an example of each of the analyzed features: Downward and upward  
 194 propagating streamers, glow, and bead. Each of the 4 sections in the figure has to the left a  
 195 281x256 pixel (6.7x6.1 degrees field of view) sub-image extracted from the original image, and  
 196 to the right the derived spectrum. The location of the sprite feature (the zero order spectrum) is  
 197 given by the white vertical lines at top and bottom of each image. The feature and associated  
 198 spectrum is bracketed by two white dashed horizontal lines which define the section of the  
 199 columns over which we integrated to get the spectral signal. The number of pixels in the section,  
 200 typically between 3 and 6, was set individually for each sequence to optimize the quality of the  
 201 derived spectra. (The horizontal lines also have a small slant to compensate for the grating not  
 202 being exactly aligned with the rows in the spectrograph CCD). The first order spectrum is seen  
 203 toward the right in the sub-image. The second order spectrum would be located farther to the  
 204 right and outside the sub-image, but is rarely detected. In the panel to the right of the image we  
 205 show the spectrum derived by summing image pixel values in each image column between the  
 206 two horizontal lines. The spectrum is wavelength scaled using 4.05 nm/pixel, as derived from a  
 207 wavelength calibration, and the location of the zero order spectrum as origin. To allow easy  
 208 visual comparison between individual spectra within a sequence and between sequences, we  
 209 scaled all spectra to a fixed amplitude of the  $\Delta v=3$  bands of the 1P system of molecular nitrogen.  
 210 The blue section covers the wavelength range 380-450 nm and is shown in blue. The red section,  
 211 625-700 nm, is shown in red.

212 In the 4 examples presented in figure 1 we note that blue emissions, indicating a more  
 213 energetic process, are only prominent in streamer spectra (upper row of figure 1). This is  
 214 generally true for the entire data set analyzed. The downward and upward streamer examples in  
 215 Figure 1 are from the same event (same image used in the figure). However, when comparing the  
 216 two spectra, or any set of spectra from other events, quenching, which is altitude dependent,  
 217 must be considered.



218

219 **Figure 1.** Examples of spectra: Downward and upward propagating streamers, glow, and bead.  
 220 Note the example of downward and upward propagating streamers are from the same event. The  
 221 spectra are normalized to the  $\Delta v=3$  band of the 1P system in the red to allow easy visual

222 comparison with the more energetic 2P system and the 1NN2+ emissions in the blue. Note  
 223 Jupiter in the field of view of the sprite in the lower right panel.

#### 224 4.1 Uncertainty on altitude

225 The altitude of the emitting sprite feature is typically calculated from the elevation angle  
 226 of the feature together with the range to the sprite. The high-speed camera had a co-aligned low-  
 227 light-level video camera which provides good star fields from which the elevation angle to the  
 228 sprite feature can be accurately determined, and the range is given by assuming that the sprite is  
 229 at the same distance from the aircraft as the causal lightning strike recorded by NLDN.

230 The assumption of the sprite located at the same range as the lightning strike is very  
 231 common and often, by necessity, made when observations are only available from a single site,  
 232 as is the case here. However, this may lead to significant errors. We know that sprites can be  
 233 many 10s of km from the lightning strike. Often, as in multiple C-sprite events, many sprites  
 234 appear across the camera field of view clearly indicating onset of individual sprites across a large  
 235 area. Sato et al. (2016) report sprites 8-20 km from the strikes based on observations from the  
 236 International Space Station, and Yang et al. (2015) report on a sprite more than 38 km from the  
 237 strike. Sao Sabbas et al. (2003) compared 40 triangulated sprite locations to their causal lightning  
 238 strike and found a mean distance of 40 km; the maximum distance was 82 km. Wescott et al.  
 239 (2001) presented one example where the sprite halo was centered essentially over the lightning  
 240 location, but the sprites occurred ~20 km from the strike; other triangulated sprite locations in  
 241 that study were up to 50 km from the associated strike. Finally, Lyons (1996) reported sprite  
 242 locations up to 111 km from the strike. Most of the sprites in the data set analyzed here were  
 243 observed at elevation angles between 10 and 20 degrees, and a change of 40 km in range, the  
 244 mean distance between strike and sprite reported by Sao Sabbas et al. (2003), at an elevation  
 245 angle of 15 degrees would change the altitude by 12 km. This is more than one atmospheric scale  
 246 height which would significantly affect quenching.

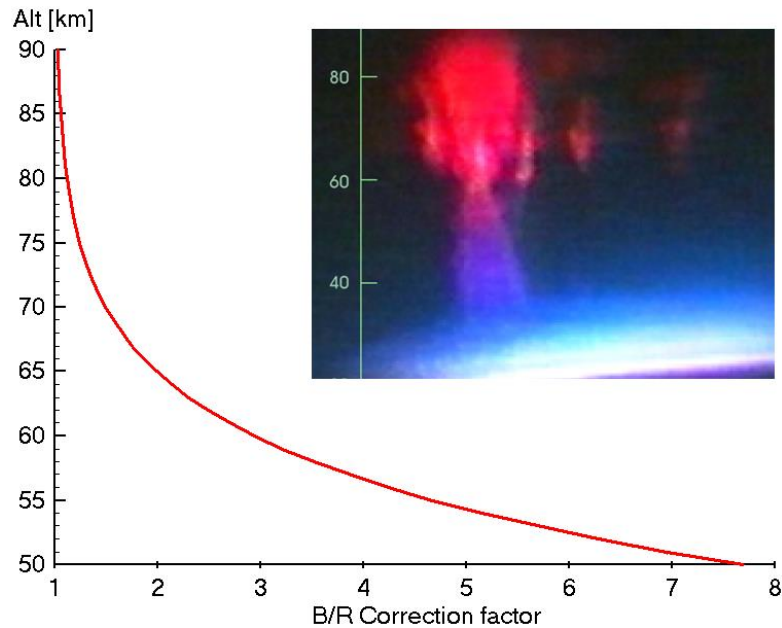
#### 247 4.2 Effect of quenching

248 Excited nitrogen molecules, neutrals and ions, may be deactivated (quenched) by  
 249 atmospheric collisions before they emit. This process becomes increasingly important at lower  
 250 altitudes. Armstrong et al. (1998), their figure 9, shows graphically the altitude effect of  
 251 quenching on the photon yield: 1P2N has a yield of 80% at 80 km decreasing to 20% at 60 km;  
 252 2PN2 is 80% at 45 km and 20% at 25 km; 1NN2+ is 80% at 60 km decreasing to 20% at 40 km.  
 253 Thus at sprite altitudes, 60-90 km, the main impact comes from quenching of the 1PN2 band  
 254 system emitting in the red. All other being equal, the blue emissions should become increasingly  
 255 prominent with lower altitude.

256 The altitude dependent increase in the observed blue/red (2PN2/1PN2) ratio due to  
 257 quenching is shown in Figure 2. The quenching ratio has been calculated using the MSIS-E-90  
 258 model atmosphere with newer emission and quenching rates given by Ihaddadene and Celestin  
 259 (2016).

260 The effect on optical sprite observations is clearly illustrated in the image inserted in  
 261 Figure 2. The image is from the first color video recording obtained by a University of Alaska  
 262 TV camera built for auroral research (Sentman et al., 1995). While the top of the sprite is red, the  
 263 color changes to blue as the red 1PN2 emissions are quenched at lower altitudes. Also

264 contributing to the lower altitude blue emissions are nitrogen ion emissions created in the  
 265 downward propagating streamer heads.



266

267 **Figure 2.** Quenching factor of the blue/red, 2PN2/1PN2, emission ratio based on the MSIS-E-90  
 268 model atmosphere with emission and quenching rates from Ihaddadene and Celestin (2016). The  
 269 inserted color image is from Sentman et al. (1995) recorded with a University of Alaska color  
 270 TV camera. It illustrates the effect of quenching. The pronounced blue bottom of the sprite is  
 271 mainly due to atmospheric quenching of the red 1PN2 emissions.

272

273

#### 4.3. Blue and Red emissions

274

275

276

277

278

279

280

281

282

283

284

285

The examples of the 4 sprite features (downward and upward propagating streamers, glow, and beads) shown in Figure 1 show that blue emissions, indicating a more energetic process, are mainly prominent in streamers. This is generally true for the entire data set analyzed. To analyze the differences more quantitatively we extracted from each spectrum the ratio between the blue emissions (380-450 nm) and red emissions (625-700 nm). Then to establish a characteristic B/R ratio for each of the 50 time series we averaged the ratios within each time series. Then we averaged the averages within each of the 4 sprite features, downward and upward propagating streamers, glows, and beads. Because of the uncertainty on the quenching correction introduced by the assumption of the sprite features located at the same range as the causal lightning strike, we give the statistics for both the observed B/R ratios and the quenching corrected values. The ratios are not corrected for instrument response or atmospheric effects. A summary of the data is given in Table 1.

286

287

288

289

	Downward streamer	Upward streamer	Glow	Bead
Number of time-series	18	6	12	14
Number of spectra in each	4-21	3-11	5-70	4-77
Observed B/R ratio range	0.058-0.300	0.018-0.164	0.004-0.114	0.000-0.053
Average obs. B/R ratio	0.178	0.077	0.034	0.013
Corrected B/R ratio range	0.010-0.179	0.013-0.092	0.003-0.051	0.000-0.020
Average corr. B/R ratio	0.055	0.047	0.017	0.006
Median corrected B/R ratio	0.050	0.057	0.013	0.006

290

291 **Table 1.** Summary of data set. Line 1: Number of time-series in each of the 4 sprite features.  
 292 Line 2: Range of the number of spectra in each sequence, e.g. the number of spectra in the 18  
 293 downward streamer sequences vary from 4 to 21. Line 3: Range of averaged ratios within each  
 294 of the 4 sprite features. Line 4: Average of the entries in line 3. Line 5 has the quenching  
 295 corrected ratio ranges and line 6 the corresponding averages. Last line, line 6, has the median of  
 296 the quenching corrected averages.

297

298 The summary confirms that the blue emissions are primarily associated with streamers.  
 299 The average quenching corrected B/R ratios for downward propagating streamers is larger than  
 300 the ratio for upward propagating streamers, as would be expected from models (e.g. Babaeva and  
 301 Naidis, 1997; Liu and Pasko, 2004; Luque et al., 2008; Qin and Pasko, 2014), but the difference  
 302 is small and well within the uncertainty on the analysis. The B/R ratios for glow and beads are  
 303 low. In several of the bead time series analyzed there were no blue emissions detected. Also, in  
 304 contrast to the streamers, glow and beads are essentially stationary and longer lasting, and  
 305 consequently, their time series are generally significantly longer.

306 The largest quenching correction to the observed B/R ratios is for downward streamers.  
 307 This is not surprising since downward streamers generally propagate to altitudes lower than  
 308 upward streamers, glow, and beads. With the quenching correction we find the average ratio of  
 309 downward streamers slightly larger than that of upward streamers in qualitative agreement with  
 310 streamer models. We tried different assumptions for deriving the altitudes to see the impact on  
 311 the quenching corrected emission ratios. Pasko and Stenbaek-Nielsen (2002) suggested that the  
 312 change to very diffuse emissions often seen in the top of carrot sprites around 80 km altitude is  
 313 associated with a sharp increase in conductivity at the edge of the ionosphere. This  
 314 morphological boundary is very easy to identify when present. Another method is to set the  
 315 altitude for a given sprite feature, and then adjust the range accordingly. The different  
 316 assumptions significantly affects the ratios in individual spectral time series, but surprisingly, the  
 317 average quenching corrected B/R ratio for downward streamers remains slightly higher than that  
 318 for the upward streamers. Nevertheless, the uncertainty on the ratios remains substantial.

319

#### 320 4.4. Temporal variations in blue and red emissions

321 The statistical analysis presented in the previous section showed the more energetic  
 322 nature of streamers relative to glow and beads. We now turn to an evaluation of individual

323 spectral time series to extract information about general systematic temporal changes in the  
324 spectra from each of the 4 small scale sprite features considered.

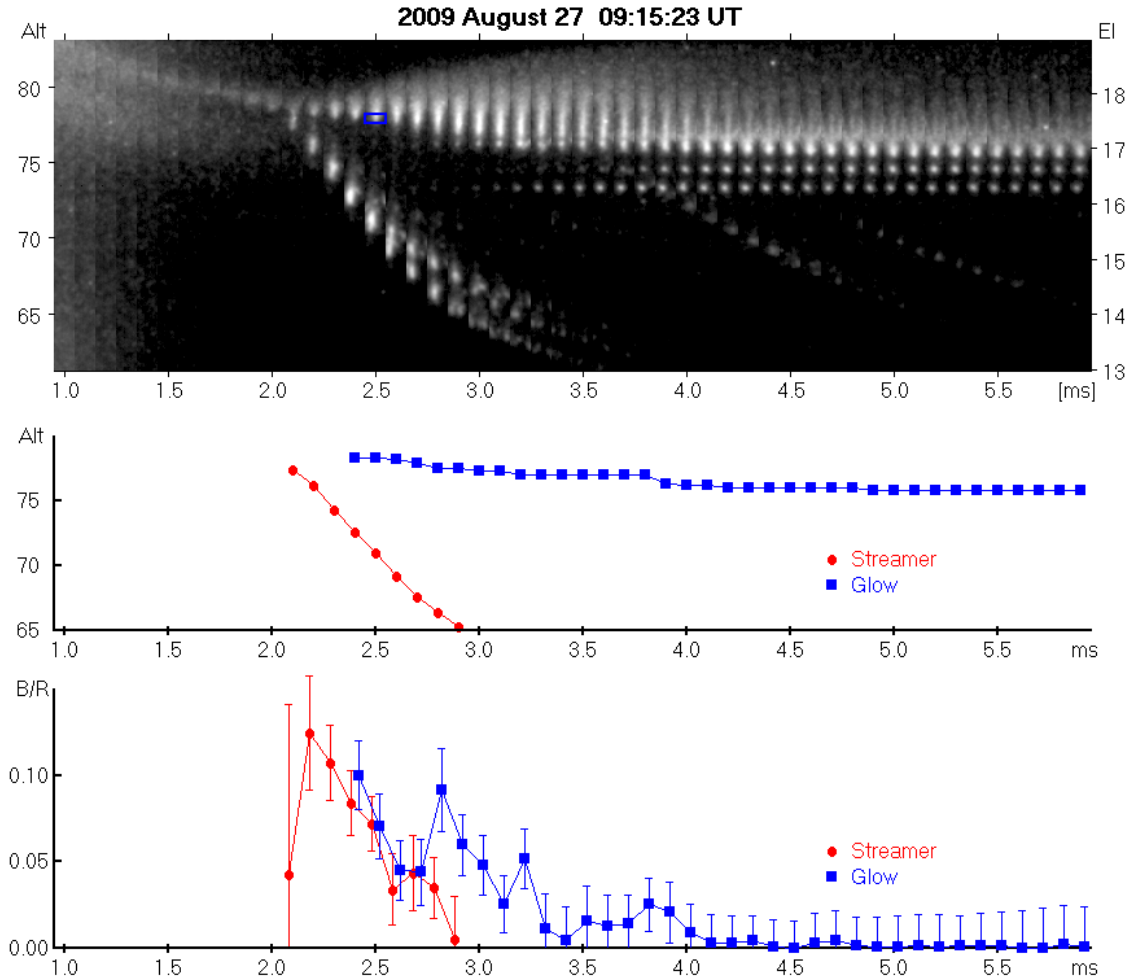
325 Temporal changes in the blue to red ratio may indicate a change in the electron energies  
326 leading to the emissions. The blue to red ratio is affected by quenching which is altitude  
327 dependent reflecting the exponentially increasing atmospheric density with lower altitude (Figure  
328 2). The effect is particularly important in downward streamers as they can propagate through  
329 several scale heights. We corrected the ratios for quenching by assuming that the range to the  
330 emitting sprite feature is the same as to the causal lightning strike reported by NLDN  
331 recognizing, as described in sections 4.1 and 4.2 above, the significant uncertainty associated  
332 with this assumption. The quenching correction will remove ratio changes within individual time  
333 series solely due to the changing altitude. If a different range is used the altitudes of all data  
334 points within the time series will change to higher or lower altitudes obviously affecting the  
335 quenching correction, but any temporal changes to the ratios within the individual time series  
336 due to processes other than quenching will remain. Thus relative changes in the quenching  
337 corrected ratios may indicate a change in the energy of the electrons responsible for the  
338 emissions.

339 The sprite shown in the lower right panel of Figure 1 provided spectral time series for a  
340 downward streamer, glow, and two beads, and we show data from this event in Figure 3. The  
341 sprite has been discussed earlier by Kanmae et al. (2010b) and by Stenbaek-Nielsen et al. (2013).  
342 It is a small and not very bright carrot recorded on 27 August 2009 at 09:15:23 UT over  
343 Oklahoma in the US Mid-West. The event has Jupiter in the field of view and we use the  
344 standard deviation observed in the Jupiter spectra (see section 3 above) to estimate error bars on  
345 the spectral ratios derived.

346 The top panel of Figure 3 has a series of 50 tall and narrow image strips, 5 ms of time,  
347 extracted from the original images to illustrate the morphology. The image used in Figure 1 is at  
348 4.2 ms in Figure 3. The altitude scale is on the left and the elevation angle scale on the right.  
349 Luminosity from the causal lightning strike was observed 1.0 ms (10 frames) before the start of  
350 the strip image time series plot, and we use that for timing. An elve propagated down across the  
351 field of view following the lightning strike, and a sprite halo appeared in the high speed images  
352 0.3 ms after the lightning strike. The panel starts with the first indication of a local intensification  
353 within the halo eventually leading to streamer formation at 2.0 ms.

354 The sprite has usable spectra for the downward propagating streamer dominating the left  
355 part of the panel, the associated glow in the top half of the panel, and the two well-defined beads  
356 below the glow. The assumed altitudes of the spectra of the streamer and glow are shown in the  
357 middle panel, and the quenching corrected blue/red ratios are shown in the bottom panel. We  
358 have not plotted data points for the beads since their altitudes do not vary and essentially no blue  
359 emissions are present in the bead spectra.

360



361  
 362 **Figure 3.** Sprite observed 27 August 2009 at 09:15:23 UT over Oklahoma. The top panel has an  
 363 image time series starting with the first indication of an intensification leading to streamer  
 364 formation. The image time series has several streamers, glow and beads. Spectra of the dominant  
 365 streamer and the glow above were extracted from a narrow altitude range (range for the glow is  
 366 indicated with a blue box at 2.5 ms). The middle panel shows the altitudes the streamer (in red)  
 367 and the glow (in blue). The bottom panel has the quenching corrected blue to red emission ratios  
 368 derived from the observed spectra with associated error bars. The time axis is ms from the  
 369 lightning/elve associated with the sprite. The data points for the streamer and glow ratios have  
 370 been slightly offset to avoid overlapping error bars.

371

372 At start of the image time series an intensification in the halo is seen moving slowly  
 373 down at  $0.3 \cdot 10^7$  m/s leading to streamer initiation around 2.1 ms. The spectra for the  
 374 intensification are very noisy, but there are no obvious blue emissions attributable to the  
 375 intensification. At the start of the downward propagating streamer blue emissions appear and  
 376 there is a rapid increase in both streamer brightness and in the blue/red ratio consistent with  
 377 modeling by Liu et al. (2009b). The maximum streamer brightness is near 2.5 ms at which time a  
 378 split is observed. The downward velocity of the streamer is initially  $1.7 \cdot 10^7$  m/s, but starts to  
 379 decrease shortly after the split. The blue/red ratio also decreases rapidly as the streamer

380 propagates down. The end of usable streamer spectra is at 2.9 ms, but the streamer is clearly  
381 visible beyond that time. It slows down and fades near the bottom of the field of view.

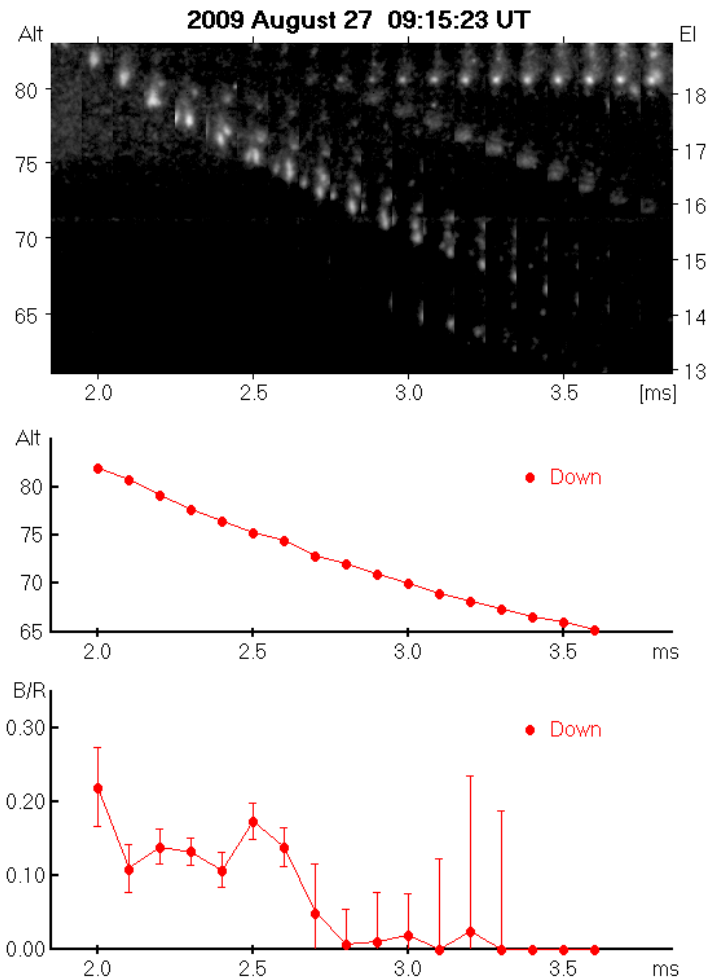
382       Bright, stationary glow and beads form after streamer onset near the altitude of the onset.  
383 In the strip image time series the glow appears as a continuation of the intensification in the halo  
384 leading to the streamer initiation. The glow spectra plotted start 2 frames from the streamer onset  
385 and the entire glow spectral time series has 80 data points. This is 4.5 ms beyond the time  
386 covered in Figure 3. The glow expands both up and down and the spectra are from the lower tip  
387 of the glow which is the best defined small feature in the glow. The location at 2.5 ms is shown  
388 with a blue box on the strip image in Figure 3 (top panel). There is a faint bead early in the time  
389 series at an altitude of 76 km; it brightens as the glow expands down over the bead (which causes  
390 the small ‘jump’ in the altitude of the spectra at 3.8 ms). We see this development quite often in  
391 our high speed sprite recordings although in this case the bead remains distinct to the end of the  
392 time series.

393       The blue/red ratio for the glow is initially similar to that for the streamer, and it decreases  
394 as the streamer fades. There is a slight increase in the ratio starting around 3.5 ms, which is likely  
395 associated with additional streamer activity. For most of the glow, from 3.0 ms until the end of  
396 the time series at 9.3 ms, very little blue is detected. This is quite representative of our data;  
397 when blue emissions are present, they appear to be associated with streamer activity early in the  
398 sprite event.

399       Below the glow there are two well defined beads which formed in the streamer channel  
400 some tenths of milliseconds after the streamer passage. This is very typical of sprite bead  
401 formation (Luque et al., 2016, Stenbaek-Nielsen et al., 2013). As mentioned above we do not  
402 show the data for the beads in the lower panels of Figure 3 since there are essentially no blue  
403 emissions detected.

404       The downward propagating streamer in Figure 3 fades near the bottom of the field of  
405 view, but there are no usable spectra covering the fade. However, we do have spectra covering  
406 the fade of another downward propagating streamer in the same event. The streamer enters the  
407 field of view from above slightly left of the streamer in Figure 3 and 0.1 ms earlier. Data for this  
408 streamer is presented in Figure 4 using the same format as for Figure 3. Initially there are  
409 significant blue emissions, but towards the end, as the streamer fades, the blue/red ratio  
410 decreases to near zero. We see that too in other time series covering streamer fade. We do not  
411 plot the estimated error for the last three data points; the streamer is here very faint and error  
412 estimation becomes meaningless.

413



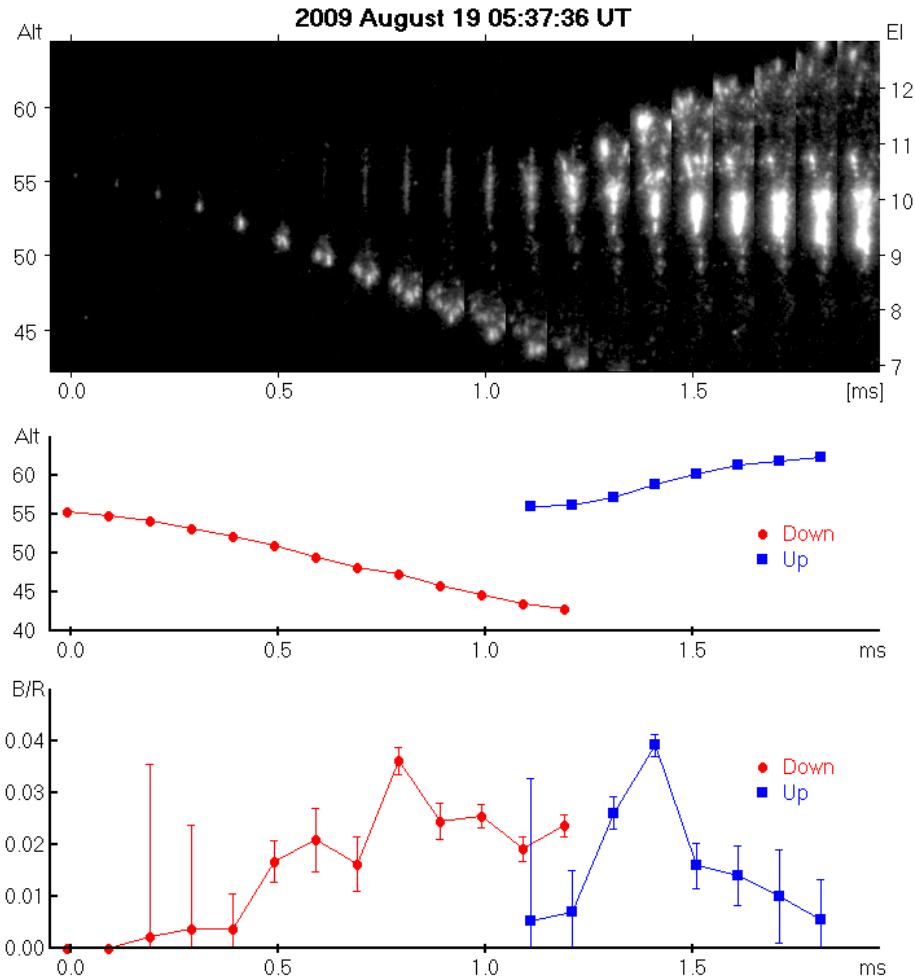
414 **Figure 4.** Sprite observed 27 August 2009 at 09:15:23 UT over Oklahoma (from the same event  
 415 as shown in Figure 3). The top panel has an image time series starting at the time the streamer  
 416 comes into view. The middle panel shows the altitude of the streamer and the bottom panel has  
 417 the corresponding quenching corrected blue to red emission ratios derived from the spectra. The  
 418 time axis is ms from the lightning/elve associated with the sprite.  
 419

420

421 The initial ratios in the streamer are higher than those shown in Figure 3, but this is very  
 422 likely an artifact of the assumption that all features in the images are at the same range. The  
 423 streamer initiates in the halo as did the streamer in Figure 3, but it is higher in the Phantom field  
 424 of view indicating a higher altitude which leads to a smaller quenching correction. A more likely  
 425 interpretation is that the streamer originates closer to the aircraft and therefore higher in the field  
 426 of view, but not higher in altitude. If we set the range so the onset altitude is the same as used for  
 427 the streamer in Figure 3, the blue/red ratios will be similar to the values shown in Figure 3.

428 Our data set has 18 time series of downward propagating streamers with 12 spectral time  
 429 series covering streamer onset and most, 8 of the 12, have onset against a dark sky. For these  
 430 streamers, in contrast to the streamer shown in Figure 3, the streamer brightness and downward  
 431 velocity increases gradually. An example is shown in Figure 5 using the same format as Figure 3.  
 432 This sprite was observed on 19 August, 2009, at 05:37:36 UT west of Oklahoma City. We do not

433 have any indication of the causal lightning strike in the high speed images (luminosity from the  
 434 strike or an elve). NLDN does report the strike, but only with 100 ms time resolution, so we use  
 435 the first indication of the downward propagating streamer for timing. The event has no stars  
 436 present that can be used to estimate the error on and confidence in the derived blue/red ratios, but  
 437 the instrument settings are similar and we use the Jupiter spectra used for the event in Figures 3  
 438 and 4.



439  
 440

441 **Figure 5.** Sprite observed on 2009 August 19 at 05:37:36 UT over Western Oklahoma. The top  
 442 panel has 20 narrow strips extracted from the Phantom images. The image time series shows the  
 443 development of a downward propagating streamer with onset against a dark sky followed by an  
 444 upward propagating streamer. The center panel has the altitudes of the downward propagating  
 445 streamer in red and the upward propagating streamer in blue. The bottom panel shows the  
 446 corresponding blue/red ratios derived from the observed spectra. The data points for the blue/red  
 447 ratios have been slightly offset to avoid overlapping error bars at 1.1 ms.

448

449 The streamer is initially very faint and the first two data points are included to illustrate  
 450 the gradual brightness and velocity increase of the streamer. No blue emissions were detected  
 451 and because of the low brightness we do not estimate the error. As the streamer brightens the

452 downward velocity increases gradually from  $0.5 \cdot 10^7$  m/s at onset to a maximum of  $1.5 \cdot 10^7$  m/s.  
 453 The blue/red ratio is low at onset, but increases after 4 frames. The streamer never becomes very  
 454 bright, and it exits the imager field of view at 1.3 ms.

455 The event in Figure 5 also has an example of an upward propagating streamer with usable  
 456 spectra. This is one of 6 in the total data set. The sequences of upward streamers generally  
 457 consist of fewer frames, and the red and blue spectral features used for the analysis are often  
 458 poorly defined because of the presence of other activity nearby. Essentially, well-defined spectra  
 459 are recorded only for streamers propagating up above the glow and activity in the onset region as  
 460 in the example in Figure 1. Our best example is the one shown in figure 5. At streamer onset and  
 461 towards the end there is less light detected in the blue. The first detection of the upward streamer  
 462 is at 0.8 ms, but spectra are only usable from 1.1 ms. There are splits in the streamer, and this  
 463 example does not end with a diffuse cloud at the top as is most often observed. The maximum  
 464 upward velocity is  $1.7 \cdot 10^7$  m/s slightly higher than the maximum velocity,  $1.5 \cdot 10^7$  m/s, in the  
 465 downward streamer in the figure consistent with earlier analysis results by McHarg et al. (2007),  
 466 Li and Cummer (2009), and Stenbaek-Nielsen et al. (2013).

467

## 468 **5 Discussion**

469 The ratio of the molecular nitrogen emissions in the blue (2PN2) to the red emissions  
 470 (1PN2) with appropriate corrections for instrument response, quenching, and atmospheric  
 471 absorption were originally intended to be used to verify sprite model results. However, as  
 472 discussed in this paper, the assumption of the sprite located at the same range as the causal  
 473 lightning strike introduces significant uncertainty on the derived altitudes, and therefore on the  
 474 quenching correction. To illustrate this we may look at the spectra from the downward and  
 475 upward propagating streamers shown in the top row of Figure 1. The two spectra are from the  
 476 same event observed over southern Nebraska on 2 August 2013 at 06:57:20 UT. The observed  
 477 blue to red ratio for the downward streamer (Figure 1 top left) is 0.36 and 0.13 for the upward  
 478 streamer (Figure 1 top right). The corresponding altitudes, assuming the same range as the causal  
 479 lightning strike, are 56.2 and 83.3 km, and correcting for quenching (Figure 2) the ratios become  
 480 0.09 and 0.12. This would indicate the upward streamer to be more energetic than the downward  
 481 streamer, in conflict with modeling by Liu and Pasko (2004) and Liu et al. (2014). If the range is  
 482 increased by for example 40 km, the mean distance between the sprite and the causal lightning  
 483 strike reported by Sao Sabbas et al., (2003), the altitudes for the two features would increase  
 484 leading to quenching corrected ratios of 0.14 and 0.12; the downward streamer is now the more  
 485 energetic.

486 The large uncertainty clearly shows the need for better sprite altitude determination. An  
 487 obvious solution is to have multiple stations so the sprite altitudes can be derived by  
 488 triangulation. Another possibility would be to avoid using the 1PN2 band emissions which are  
 489 most affected by quenching. Modeling by Pérez-Invernón et al. (2018) indicate that the ratio of  
 490 2PN2 to 1NN2+ can be used, but these optical bands are both in the blue and may be difficult to  
 491 separate in slit-less spectroscopic data. This problem can be overcome by adding narrow band  
 492 filtered imagers to augment the spectral images. Observations using multiple imagers with  
 493 narrow band optical filters were used in some of the early aircraft observations (Morrill et al.,  
 494 2002; Armstrong et al., 2000) and is used in current observations from the International Space  
 495 Station (Neubert et al., 2019).

496 While the blue to red nitrogen emission ratios derived are associated with large  
497 uncertainties, we note that just the presence of blue emissions will indicate a more energetic  
498 process. The analysis presented here shows that blue emissions are primarily associated with  
499 streamer processes early in a sprite event. This supports the suggestion made in the early years of  
500 sprite research by Suszcynsky et al. (1998) and Armstrong et al. (2000) that there are two  
501 separate mechanisms associated with the sprite emissions: An initial energetic process, which we  
502 here identify as associated with streamer activity, followed by less energetic processes associated  
503 with the much longer lasting glow and bead sprite features.

504 Analysis of the streamer spectra shows temporal changes in the blue to red emissions  
505 ratios within individual time series indicating corresponding changes in the energy of the  
506 electrons leading to the emissions. The data set has 18 time series of downward propagating  
507 streamers with 12 covering streamer onset. Of the 12, 4 have onset in or near a sprite halo and 8  
508 have onset against a dark sky.

509 The 4 time series with onset in or near a sprite halo are prompt sprites with streamer  
510 onset within a few ms of the causal lightning strike. The streamer brightness and velocity  
511 increases very rapidly, and they emerge from the halo with blue to red ratio and downward  
512 velocity near the maximum observed for that individual streamer. The maximum downward  
513 velocity in the 4 streamers is in the range  $1.5\text{-}2.5 \cdot 10^7$  m/s. An example was presented above in  
514 Figure 3.

515 The 8 streamers with onset against a dark sky are all delayed sprites with onset 50-300  
516 ms after the lightning strike. In contrast to the rapid brightening and high initial downward  
517 velocity observed in the prompt streamers, the brightness and downward velocity increase  
518 gradually, typically over about 0.5 ms (5 frames). An example was presented in Figure 5 above.  
519 Similar examples (but without spectral information) may also be found in Stenbaek-Nielsen et al.  
520 (2010). The maximum downward velocity in the 8 streamers is in the range  $1.0\text{-}2.0 \cdot 10^7$  m/s,  
521 slightly less than the downward velocity range for the prompt streamers. The delayed sprites  
522 appear to have their onset at a lower altitude than the prompt sprites as has been reported by Li et  
523 al. (2008) who quote a 5 km altitude difference.

524 Towards the end of the downward propagation the streamer gradually fades. The  
525 streamer fade is covered in 8 of the 18 time series. The fade is often associated with a decrease in  
526 downward velocity, but the decrease varies considerably between events and does not appear to  
527 be obviously associated with the decrease in streamer brightness. An example was presented in  
528 Figure 4. Li and Cummer (2012) found that the streamers begin their significant deceleration  
529 where the background field drops below 12–24 % of the local electric break-down field,  $E_k$ , and  
530 that the fade is at the altitude where the ambient E field is 5% of  $E_k$ .

531 The spectra of the upward propagating streamers appear to follow the same development  
532 with little blue emissions at the start and end of the streamers (Figure 5). However, our data set  
533 for upward streamers is very limited.

534 In sprite glow and especially in beads we find little or no blue emissions. Most of the blue  
535 emissions in glow are observed early when streamer activity is present. However, we do have  
536 examples where the blue emissions extend beyond the end of streamer activity, as determined  
537 from the high-speed images. This may indicate that the emissions may not be entirely from  
538 streamers within the region of the glow, and we suggest that they may be associated with  
539 currents in the streamer channels as first proposed by Lui (2010) and later by Luque et al. (2016).

540 Luque et al. (2016) showed that glow and beads in the same streamer channel decay with the  
 541 same time constant even though they were several scale heights apart in altitude indicating a  
 542 coupling of the processes within the channel. They suggested a model in which the emissions in  
 543 the glow and beads are produced by the same process driven by the current in the channel. The  
 544 local E-field in the channel is dictated by the current which through an electron attachment  
 545 instability drives the local plasma in the channel into one of two states: a high conductivity state  
 546 resulting in a low E-field and no optical emissions, or, a low conductivity state resulting in a high  
 547 E-field and optical emissions which would be the channel glow and beads. The E-field in this  
 548 model is naturally limited to the local field required for ionization,  $E_k$ ; if the field locally  
 549 increases above  $E_k$  ionization would occur increasing the conductivity and consequently, with  
 550 the current being constant the local E-field in the channel would decrease. As the sprite decays  
 551 the current decreases and the E-field would decrease as well. Eventually there will be only 1P  
 552 emissions present. As the current decay further there will be no optical emissions, but the  
 553 channel will remain providing a seed for sprite re-ignition as is often observed (Stenbaek-Nielsen  
 554 et al., 2000; 2013; Sentman et al., 2008).

555

## 556 Acknowledgments

557 We gratefully acknowledge the support of the NSF/NCAR High Performance Instrumented  
 558 Airborne Platform for Environmental Research (HIAPER) project, as well as the pilots and  
 559 technical staff that made the HIAPER Gulfstream V missions possible. We also acknowledge the  
 560 contribution by T. Kanmae who did the early analysis of the spectra, and discussions with N.  
 561 Liu, F. J. Pérez-Invernón, and A. Malagón-Romero. The data presented here are available on  
 562 Open Science Framework (<https://osf.io>) in project “Sprite Spectra at 10,000 fps”. The data are  
 563 also available from H. Stenbaek-Nielsen ([hcn Nielsen@alaska.edu](mailto:hcn Nielsen@alaska.edu)) or M.G. McHarg  
 564 ([Matthew.McHarg@usafa.edu](mailto:Matthew.McHarg@usafa.edu)). The research has been supported in part by NSF grants 1104441  
 565 to the University of Alaska Fairbanks and 1201683 to the US Air Force Academy.

566

## 567 References

- 568 Armstrong, R. A., Shorter, J. A., Taylor, M. J., Suszcynsky, D. M., Lyons, W. A., & Jeong, L. S.  
 569 (1998). Photometric measurements in the SPRITES '95 & '96 campaigns of nitrogen second  
 570 positive (399.8 nm) and first negative (427.8 nm) emissions. *Journal of Atmospheric and*  
 571 *Solar-Terrestrial Physics*, 60(7–9), 787–799. [https://doi.org/10.1016/S1364-6826\(98\)00026-](https://doi.org/10.1016/S1364-6826(98)00026-1)  
 572 1
- 573 Armstrong, R. A., Suszcynsky, D. M., Lyons, W. A., & Nelson, T. E. (2000). Multi-color  
 574 photometric measurements of ionization and energies in sprites. *Geophysical Research*  
 575 *Letters*, 27(5), 653–656. <https://doi.org/10.1029/1999GL003672>
- 576 Babaeva, N. Y., & Naidis, G. V. (1997). Dynamics of positive and negative streamers in air in  
 577 weak uniform electric fields. *IEEE Transactions of Plasma Science*, 25, 375–9.  
 578 <https://doi.org/10.1109/27.602514>
- 579 Cartwright, D. C. (1978). Vibrational populations of the excited states of  $N_2$  under auroral  
 580 conditions. *Journal of Geophysical Research*, 83(A2), 517–531.  
 581 <https://doi.org/10.1029/JA083iA02p00517>

- 582 Cummer, S. A., Jaugey, N., Li, J., Lyons, W. A., Nelson, T. E., & Gerken, E. A. (2006).  
 583 Submillisecond imaging of sprite development and structure. *Geophysical Research Letters*,  
 584 33, L04104. <https://doi.org/10.1029/2005GL024969>
- 585 Gordillo-Vázquez, F. J., Passas, M., Luque, A., Sánchez, J., van der Velde, O. A., & Montanyà, J.  
 586 (2018). High spectral resolution spectroscopy of sprites: A natural probe of the mesosphere.  
 587 *Journal of Geophysical Research: Atmospheres*, 123, 2336–2346.  
 588 <https://doi.org/10.1002/2017JD028126>
- 589 Hampton, D. L., Heavner, M. J., Wescott, E. M., & Sentman, D. D. (1996). Optical spectral  
 590 characteristics of sprites. *Geophysical Research Letters*, 23(1):89–92.  
 591 <https://doi.org/10.1029/95GL03587>
- 592 Ihaddadene, M. A., & Celestin, S. (2017). Determination of sprite streamers altitude based on N<sub>2</sub>  
 593 spectroscopic analysis. *Journal of Geophysical Research: Space Physics*, 122, 1000–1014.  
 594 <https://doi.org/10.1002/2016JA023111>
- 595 Kanmae, T., Stenbaek-Nielsen, H. C., & McHarg, M. G. (2007). Altitude resolved sprite spectra  
 596 with 3 ms temporal resolution. *Geophysical Research Letters: Space Physics*, 34, L07810.  
 597 <https://doi.org/10.1029/2006GL028608>
- 598 Kanmae, T., Stenbaek-Nielsen, H. C., McHarg, M. G., & Haaland, R. K. (2010a). Observation of  
 599 sprite streamer head's spectra at 10,000 fps. *Journal of Geophysical Research*, 115, A00E48.  
 600 <https://doi.org/10.1029/2009JA014546>
- 601 Kanmae, T., Stenbaek-Nielsen, H. C., McHarg, M. G., & Haaland, R. K. (2010b). Observation of  
 602 blue sprite spectra at 10,000 fps. *Geophysical Research Letters*, 37, L13808.  
 603 <https://doi.org/10.1029/2010GL043739>
- 604 Kuo, C.-L., Hsu, R. R., Chen, A. B., Su, H. T., Lee, L. C., Mende, S. B., Frey, H. U., Fukunishi,  
 605 H., & Takahashi, Y. (2005). Electric fields and electron energies inferred from the ISUAL  
 606 recorded sprites. *Geophysical Research Letters*, 32, L19103.  
 607 <https://doi.org/10.1029/2005GL023389>
- 608 Li, J., Cummer, S. A., Lyons, W. A., & T. E. Nelson (2008). Coordinated analysis of delayed  
 609 sprites with high-speed images and remote electromagnetic fields. *Journal of Geophysical*  
 610 *Research: Atmospheres*, 113, D20206. <https://doi.org/10.1029/2008JD010008>
- 611 Li, J., & Cummer, S. A. (2009). Measurement of sprite streamer acceleration and deceleration.  
 612 *Geophysical Research Letters*, 36, L10812. <https://doi.org/10.1029/2009GL037581>
- 613 Li, J., & Cummer, S. (2012). Relationship between sprite streamer behavior and lightning-driven  
 614 electric fields. *Journal of Geophysical Research: Space Physics*, 117, A01317.  
 615 <https://doi.org/10.1029/2011JA016843>
- 616 Liu, N. Y. (2010). Model of sprite luminous trail caused by increasing streamer current.  
 617 *Geophysical Research Letters*, 37, L04102. <https://doi.org/10.1029/2009GL042214>
- 618 Liu, N. Y., & Pasko, V. P. (2004). Effects of photoionization on propagation and branching of  
 619 positive and negative streamers in sprites. *Journal of Geophysical Research: Space Physics*,  
 620 109, A04301. <https://doi.org/10.1029/2003JA010064>.
- 621 Liu, N. Y., Pasko, V. P., Burkhardt, D. H., Frey, H., Mende, S., Su, H.-T., Chen, A., Hsu, R. R.,  
 622 Lee, L.-C., Fukunishi, H., & Takahashi, Y. (2006). Comparison of results from sprite  
 623 streamer modeling with spectrophotometric measurements by ISUAL instrument on  
 624 FORMOSAT-2 satellite. *Geophysical Research Letters*, 33, L01101.  
 625 <https://doi.org/10.1029/2005GL024243>
- 626 Liu, N. Y., Pasko, V. P., Frey, H., Mende, S., Su, H.-T., Chen, A., Hsu, R. R., & Lee, L.-C.  
 627 (2009a). Assessment of sprite initiating electric fields and quenching altitude of a1Pg state of

- 628 N<sub>2</sub> using sprite streamer modeling and ISUAL spectrophotometric measurements. *Journal of*  
 629 *Geophysical Research: Atmospheres*, 114, A00E02. <https://doi.org/10.1029/2008JA013735>
- 630 Liu, N. Y., Pasko, V. P., Adams, K., Stenbaek-Nielsen, H. C., & McHarg, M. G. (2009b).  
 631 Comparison of acceleration, expansion, & brightness of sprite streamers obtained from  
 632 modeling and high-speed video observations. *Journal of Geophysical Research: Space*  
 633 *Physics*, 114, A00E03. <https://doi.org/10.1029/2008JA013720>
- 634 Luque, A., Ratushnaya, V., & Ebert, U. (2008). Positive and negative streamers in ambient air:  
 635 modelling evolution and velocities. *Journal of Physics D: Applied Physics*, 41, 234005  
 636 (11pp). <https://doi.org/10.1088/0022-3727/41/23/234005>
- 637 Luque, A., Stenbaek-Nielsen, H. C., McHarg, M. G., & Haaland, R. (2016). Sprite beads and  
 638 glows arising from the attachment instability in streamer channels. *Journal of Geophysical*  
 639 *Research: Space Physics*, 121, 2431-2449. <https://doi.org/10.1002/2015JA022234>
- 640 Lyons, W. (1996). Sprite observations above the U.S. high plains in relation to their parent  
 641 thunderstorm systems. *Journal of Geophysical Research: Atmospheres*, 101, 29,641–29,652.  
 642 <https://doi.org/10.1029/96JD01866>
- 643 McHarg, M. G., Stenbaek-Nielsen, H. C., & Kammer, T. (2007). Observation of streamer  
 644 formation in sprites. *Geophysical Research Letters*, 34, L06804.  
 645 <https://doi.org/10.1029/2006GL027854>
- 646 Mende, S. B., Rairden, R. L., Swenson, G. R., & Lyons, W. A. (1995). Sprite spectra; N<sub>2</sub> 1 PG  
 647 band identification. *Geophysical Research Letters*, 22(19):2633–2636.  
 648 <https://doi.org/10.1029/95GL02827>
- 649 Morrill, J., Bucsel, E., Siefring, C., Heavner, M., Berg, S., Moudry, D., Slinker, S., Fernsler, F.,  
 650 Wescott, E., Sentman, D., & Osborne, D. (2002). Electron energy and electric field estimates  
 651 in sprites derived from ionized and neutral N<sub>2</sub> emissions. *Geophysical Research Letters*,  
 652 29(10). <https://doi.org/10.1029/2001GL014018>
- 653 Neubert, T., Østgaard, N., Reglero, V., Blanc, E., Chanrion, O., Oxborrow, C. A., Orr, A.,  
 654 Tacconi, M., Hartnack, O., & Bhandari, D. V. (2019). The ASIM Mission on the  
 655 International Space Station. *Space Science Reviews*, 215:26. [https://doi.org/10.1007/s11214-](https://doi.org/10.1007/s11214-019-0592-z)  
 656 [019-0592-z](https://doi.org/10.1007/s11214-019-0592-z)
- 657 Pasko, V. P., & Stenbaek-Nielsen, H. C. (2002). Diffuse and streamer regions of sprites.  
 658 *Geophysical Research Letters*, 29(10), 82-1 to 82-4. <https://doi.org/10.1029/2001GL014241>
- 659 Pérez-Invernón, F. J., Luque, A., Gordillo-Vázquez, F. J., Sato, M., Ushio, T., Adachi, T., &  
 660 Chen, A. B. (2018). Spectroscopic diagnostic of halos and elves detected from space-based  
 661 photometers. *Journal of Geophysical Research: Atmospheres*, 123, 12,917–12,941.  
 662 <https://doi.org/10.1029/2018JD029053>
- 663 Qin, J., & Pasko, V. P. (2014). On the propagation of streamers in electrical discharges. *Journal*  
 664 *of Physics D: Applied Physics*, 47, 435202 (9pp). [https://doi.org/10.1088/0022-](https://doi.org/10.1088/0022-3727/47/43/435202)  
 665 [3727/47/43/435202](https://doi.org/10.1088/0022-3727/47/43/435202)
- 666 Taylor, J. R. (1997). An introduction to error analysis. University Science Books, Sausalito,  
 667 California.
- 668 Sao Sabbas, F., Sentman, D., Wescott, E., Pinto Jr., O., Mendes Jr., O., & Taylor, M. (2003).  
 669 Statistical analysis of space-time relationships between sprites and lightning. *Journal of*  
 670 *Atmospheric and Solar-Terrestrial Physics*, 65, 525–535. [https://doi.org/10.1016/S1364-](https://doi.org/10.1016/S1364-6826(02)00326-7)  
 671 [6826\(02\)00326-7](https://doi.org/10.1016/S1364-6826(02)00326-7)
- 672 Sato, M., Mihara, M., Adachi, T., Ushio, T., Morimoto, T., Kikuchi, M., Kikuchi, H., Suzuki,  
 673 M., Yamazaki, A., Takahashi, Y., Inan, U., Linscott, I., Ishida, R., Sakamoto, Y., Yoshida,

- 674 K. & Hobara, Y. (2016). Horizontal distributions of sprites derived from the JEM-GLIMS  
 675 nadir observations. *Journal of Geophysical Research. Atmospheres*, *121*, 3171–3194.  
 676 <https://doi.org/10.1002/2015JD024311>
- 677 Sentman, D. D., Wescott, E. M., Osborne, D. L., Hampton, D. L., & Heavner, M. J. (1995).  
 678 Preliminary results from the Sprites94 aircraft campaign: 1. Red sprites. *Geophysical*  
 679 *Research Letters*, *22*:1205. <https://doi.org/10.029/95GL00583>
- 680 Sentman, D. D., Stenbaek-Nielsen, H. C., M. G. McHarg, and J. Morrill (2008), Plasma  
 681 chemistry of sprite streamers. *Journal of Geophysical Research: Atmospheres*, *113*, D11112.  
 682 <https://doi.org/10.1029/2007JD008941>
- 683 Stanley, M., Krehbiel, P., Brook, M., Moore, C., Rison, W., & Abrahams, B. (1999). High speed  
 684 video of initial sprite development. *Geophysical Research Letters*, *26*, 3201.  
 685 <https://doi.org/10.1039/1999GL010673>
- 686 Stenbaek-Nielsen, H.C., Moudry, D.R., Wescott, E.M., Sentman, D.D., & Sao Sabbas, F.T.  
 687 (2000). Sprites and possible mesospheric effects. *Geophysical Research Letters*, *27*, 3829-  
 688 3832. <https://doi.org/10.1029/2000GL003827>
- 689 Stenbaek-Nielsen, H. C., McHarg, M. G., Kanmae, T., & Sentman, D. D. (2007). Observed  
 690 emission rates in sprite streamer heads. *Geophysical Research Letters*, *34*, L11105.  
 691 <https://doi.org/10.1029/2007GL029881>
- 692 Stenbaek-Nielsen, H. C., & McHarg, M. G. (2008). High time-resolution sprite imaging:  
 693 Observations and implications. *Journal of Physics D: Applied Physics*, *41*, 234009.  
 694 <https://doi.org/10.1088/0022-3727/41/23/234009>
- 695 Stenbaek-Nielsen, H. C., Haaland, R. K., McHarg, M. G., Hensley, B. A., & Kanmae, T. (2010).  
 696 Sprite initiation altitude measured by triangulation. *Journal of Geophysical Research: Space*  
 697 *Physics*, *115*:A00E12. <https://doi.org/10.1029/2009JA014543>
- 698 Stenbaek-Nielsen, H. C., Kanmae, T., McHarg, M. G., & Haaland, R. (2013). High-speed  
 699 observations of sprite streamers. *Survey of Geophysics*, *34*, 769–795.  
 700 <https://doi.org/10.1007/s10712-013-9224-4>
- 701 Suszcynsky, D. M., Roussel-Dupre, R., Lyons, W. A., & Armstrong, R. A. (1998). Blue-light  
 702 imagery and photometry of sprites. *Journal of Atmospheric and Solar Terrestrial Physics*,  
 703 *60*(7–9), 801–809. [https://doi.org/10.1016/S1364-6826\(98\)00027-3](https://doi.org/10.1016/S1364-6826(98)00027-3)
- 704 Vallance Jones, A. (1974). *Aurora*. D. Reidel, Dordrecht, Netherlands.  
 705 <https://doi.org/10.1007/978-94-010-2099-2>
- 706 Wescott, E.M., Stenbaek-Nielsen, H.C., Sentman, D.D., Heavner, M.T., Moudry, D.R., & Sao  
 707 Sabbas, F.T. (2001). Triangulation of sprites, associated halos and their possible relation to  
 708 causative lightning and micro-meteors. *Journal of Geophysical Research: SpacePhysics*, *106*,  
 709 10467. <https://doi.org/10.1029/2000JA000182>
- 710 Yang, J., Lu, G., Lee, L., & Feng, G. (2015). Long-delayed bright dancing sprites with large  
 711 horizontal displacement from its parent flash. *Journal of Atmospheric and Solar-Terrestrial*  
 712 *Physics*, *129*. <https://doi.org/10.1016/j.jastp.2015.04.001>
- 713